



PERGAMON

Applied Geochemistry 17 (2002) 1273–1286

www.elsevier.com/locate/apgeochem

**Applied  
Geochemistry**

# Assessing mine drainage pH from the color and spectral reflectance of chemical precipitates

David J. Williams<sup>a,\*</sup>, Jerry M. Bigam<sup>a</sup>, Charles A. Cravotta III<sup>b</sup>,  
Sam J. Traina<sup>a</sup>, John E. Anderson<sup>c</sup>, John G. Lyon<sup>d,2</sup>

<sup>a</sup>*School of Natural Resources, The Ohio State University, Columbus, OH 43210, USA*

<sup>b</sup>*US Geological Survey, Water Resources Division, New Cumberland, PA 17070, USA*

<sup>c</sup>*School of Marine Science, Virginia Institute of Marine Science, The College of William and Mary, Gloucester Point, VA 23062, USA*

<sup>d</sup>*Department of Civil and Environmental Engineering and Geodetic Science, The Ohio State University, Columbus, OH 43210, USA*

Received 11 January 2001; accepted 13 November 2001

Editorial handling by B. Kimball

## Abstract

The pH of mine impacted waters was estimated from the spectral reflectance of resident sediments composed mostly of chemical precipitates. Mine drainage sediments were collected from sites in the Anthracite Region of eastern Pennsylvania, representing acid to near neutral pH. Sediments occurring in acidic waters contained primarily schwertmannite and goethite while near neutral waters produced ferrihydrite. The minerals comprising the sediments occurring at each pH mode were spectrally separable. Spectral angle difference mapping was used to correlate sediment color with stream water pH ( $r^2=0.76$ ). Band-center and band-depth analysis of spectral absorption features were also used to discriminate ferrihydrite and goethite and/or schwertmannite by analyzing the  ${}^4T_1 \leftarrow {}^6A_1$  crystal field transition (900–1000 nm). The presence of these minerals accurately predicted stream water pH ( $r^2=0.87$ ) and provided a qualitative estimate of dissolved  $SO_4$  concentrations. Spectral analysis results were used to analyze airborne digital multispectral video (DMSV) imagery for several sites in the region. The high spatial resolution of the DMSV sensor allowed for precise mapping of the mine drainage sediments. The results from this study indicate that airborne and space-borne imaging spectrometers may be used to accurately classify streams impacted by acid vs. neutral-to-alkaline mine drainage after appropriate spectral libraries are developed. Published by Elsevier Science Ltd.

## 1. Introduction

Drainage from coal mines is one of the most important environmental legacies of industrial economies. Problems associated with coal mine drainage include sedimentation of chemical precipitates, soil erosion, loss of aquatic habitat, and the corrosion of bridge abut-

ments, culverts, and other structures due to contact with acid water having high dissolved metal loads (Albers and Camardese, 1993; Sengupta, 1993; Rosseland et al., 1990). The extensive nature of mine drainage in many regions necessitates watershed-scale assessments and prioritization of remediation efforts (Gray, 1997). A cost-effective method to identify, map, and monitor the most severely degraded mine discharges and receiving streams would benefit regulatory authorities and environmental agencies, especially in areas where rough terrain or poor roads limit accessibility.

Remote sensing has recently been used in the western USA to map mine tailings from the reflectance characteristics of mineral weathering products (Swayze et al., 2000a,b; Robbins et al., 2000). Advances in the spatial

\* Corresponding author at present address. Tel.: +1-703-648-4798; fax: +1-703-648-4290.

E-mail address: williams.davidj@epa.gov (D.J. Williams).

<sup>1</sup> Presently at US Environmental Protection Agency, Reston, VA, 20192, USA.

<sup>2</sup> Presently at US Environmental Protection Agency, Las Vegas, NV, 89119, USA.

and spectral resolution of airborne and satellite systems and improved understanding of the relation between the aqueous geochemistry and mineralogy of ochreous precipitates from mine drainage could enable the remote sensing of mine drainage quality (Anderson and Robbins, 1998; Robbins et al., 2000).

Recent studies of the ochreous precipitates from mine drainage have shown that these metal-rich deposits comprise a diverse group of minerals that form in response to fairly specific geochemical conditions (Bigham et al., 1996). Additional studies have documented a bimodal pH frequency distribution for coal mine drainage, with acidic (pH 3–4) and near neutral (pH 5.5–7.0) modes (Winland et al., 1991; Rose and Cravotta, 1998; Cravotta et al., 1999). Dissolved constituents in the mine drainage, typically Mg, Ca, Fe, Mn, Al, SO<sub>4</sub>, and HCO<sub>3</sub> (in near neutral waters) are derived from pyrite oxidation and the consequent reaction of acidic water with minerals along the flow path (Rose and Cravotta, 1998). These parameters directly influence the composition and mineralogy of downstream precipitates. The mineral precipitates from mine drainage commonly have a characteristic color and spectral reflectance depending on the geochemical environment where they formed (Williams, 1999; Anderson and Robbins, 1998; Bigham and Murad, 1997).

The purpose of this study was to (1) relate the color and spectral reflectance of mine drainage precipitates to the pH of the source waters, (2) describe how remote sensing systems can detect and map mine drainage sediments, and (3) demonstrate the importance of this knowledge to the assessment and monitoring of mine impacted watersheds.

## 2. Materials and methods

### 2.1. Study area

Mine drainage sites were investigated in the Anthracite region of eastern Pennsylvania (Wood et al., 1986). This region encompasses a 1250 km<sup>2</sup> area and extends from 30 km NE of Harrisburg to 30 km NE of Scranton, Pa. The anthracite is interbedded with folded and faulted sandstone, conglomerate, and shale of the Llewellyn and Pottsville Formations of Pennsylvanian age (320–290 Ma) (Way, 2000). Although underground and surface mining continues at a few sites, most anthracite mines were abandoned before 1960. Extensive areas of unreclaimed spoil and flooded mine voids contribute sediment and other pollutants via mine discharges to surface waters.

### 2.2. Sample collection

Sediment and water samples were collected at 9 abandoned mine discharge locations in the study area

on 15–17 October 1997 (Fig. 1). At 5 locations, mine drainage samples were taken at 3 points beginning at the mine drainage outfall, halfway between the mine drainage outfall and its confluence with a receiving stream, and immediately above the confluence. In other cases, samples were obtained at the source only (Table 1). Detailed locations for all sample sites are given in Williams (1999).

### 2.3. Multispectral imagery

Digital remote sensing imagery for several sites in the study was provided by the Virginia Institute of Marine Science (VIMS) in cooperation with the US Geological Survey (USGS). Imagery was obtained with the airborne digital multispectral video system (DMSV) (SpecTerra Systems Pty Ltd) described by Anderson and Robbins (1998). Briefly, the DMSV system collects data using a 4 charge-coupled device (CCD) array operating in the 400–900 nm range. Interchangeable filters are used to set the CCD's at specific wavelengths (nominally 450, 550, 650 and 750 nm). The mission was flown at an altitude of 1372 m and between 1000 and 1500 Eastern Standard Time.

### 2.4. Water samples

Flow rate and water-chemistry data were collected at each location according to standard methods (Wood, 1976; Rantz, 1982; Wilde et al., 1998). Volumetric discharge rates were measured at either the upstream or downstream sample site. At each sample site, specific conductance (SC), temperature, redox potential ( $E_h$ ), and dissolved O<sub>2</sub> (DO) were measured electrometrically in situ.  $E_h$  was measured with a combination Pt and Ag/AgCl electrode, checked with Zobell's solution, and corrected to 25 °C according to methods of Nordstrom (1977). Water samples were collected in 1 l polyethylene bottles and then were split into unfiltered (whole-water) and filtered subsamples and stored on ice until analyzed. Subsamples for analysis of dissolved constituents were filtered under pressure through a 0.45 µm nitrocellulose filter. Filtered and whole-water samples for analysis of metals were stored in acid-rinsed bottles and preserved with HNO<sub>3</sub>. Water samples were analyzed in the Pennsylvania Department of Environmental Protection laboratory for alkalinity, acidity, and concentrations of major ions, trace metals, and nutrients by the methods of Fishman and Friedman (1989). The total and dissolved concentrations of Al, As, Ba, Cd, Ca, Cr, Co, Cu, Fe, Pb, Li, Mg, Mn, Ni, K, Se, SiO<sub>2</sub>, Na, Sr and Zn were measured. Total concentrations of Cl<sup>-</sup>, F<sup>-</sup>, N, NH<sub>3</sub>, NO<sub>3</sub><sup>-</sup>, and SO<sub>4</sub><sup>2-</sup> were also quantified. Hydrologic and water-chemistry data for the study are published in the USGS annual water-resources data reports (Durlin and Schaffstall, 1998a,b). Total dissolved Fe and SO<sub>4</sub>

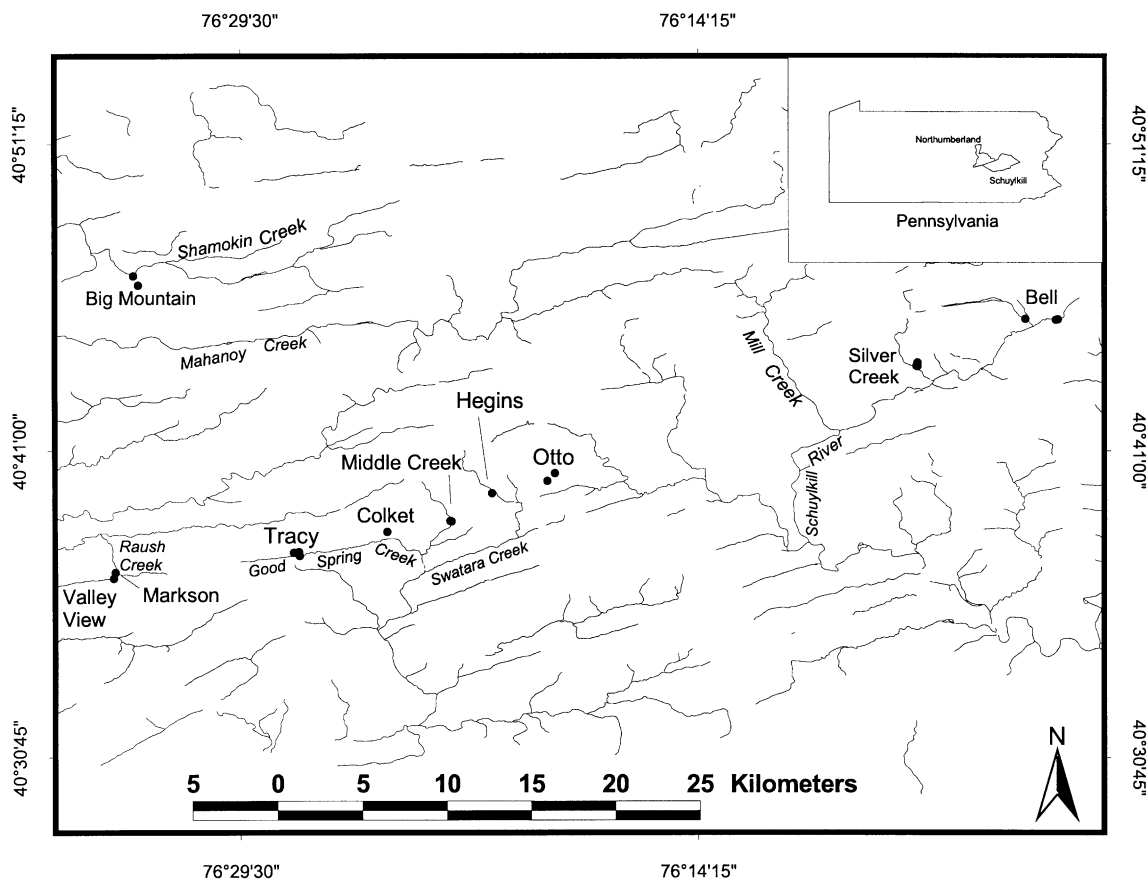


Fig. 1. Location of mine discharge sediment and water sampling sites.

concentrations were converted to activities of  $\text{Fe}^{3+}$  and  $\text{SO}_4^{2-}$  using the WATEQ4F computer program on the basis of measured temperature,  $E_h$ , pH, and concentrations of dissolved constituents (Ball and Nordstrom, 1991).

### 2.5. Sediment samples

Approximately 500 ml to 1 l of precipitate were collected in acid washed polypropylene bottles at each sampling site. At most sites, precipitates were collected by suctioning the loose floc or by removing encrustations from rocks near the perimeter of the stream bed. A battery-operated peristaltic pump was used at a few sites to suction precipitates from about 2 m depth in flooded mine shafts. All samples were placed on ice for transport to the laboratory, where they were stored at 4 °C. After the sediments settled, the supernatant liquids were decanted and discarded. The precipitates were then wet sieved through a 60-mesh stainless steel sieve, and the detrital material was discarded. The precipitates were then concentrated by centrifugation, washed by dialysis against deionized  $\text{H}_2\text{O}$ , quick frozen in liquid

$\text{N}_2$ , and freeze-dried in a Labconco lyophilizer at room temperature.

#### 2.5.1. Mineralogical analysis

Mineralogy was determined using powder X-ray diffraction (XRD). Freeze-dried precipitates were crushed, placed in a backfill powder mount, and scanned using  $\text{CuK}\alpha$  radiation with a Philips PW1070 diffractometer equipped with a diffracted beam monochromator and a 1° divergence slit. Samples were step scanned from 10 to 80°  $2\theta$  in increments of 0.01°  $2\theta$  with a 4 s counting time.

#### 2.5.2. Color measurements and analysis

Color was measured for the freeze-dried sediment samples using a Minolta CR-300 Chroma Meter, a portable tristimulus color analyzer used for analyzing the reflective colors of materials. The chroma meter was first calibrated using red, yellow, and white color plates. Freeze-dried samples were then pressed to create an opaque surface. The reflectance values were collected and both Munsell and  $L^*a^*b^*$  color parameters were calculated for each sample. Conversion of  $L^*a^*b^*$  to

Table 1  
Mineralogy and color of sediment samples, elemental composition of the acid-soluble (5M HCl) fraction, and source water pH, SC and dissolved sulfate

Site	Distance from source (m)	Mineralogy <sup>a</sup>	Acid soluble fraction									Source water						
			Fe	Si	Al	Mn	SO <sub>4</sub>	Fe <sub>tot</sub> /S <sub>tot</sub>	CIE color			Munsell color			pH	SC μScm <sup>-1</sup>	SO <sub>4</sub> mmol/l	
									L*	a*	b*	Hue	Value	Chroma				
Bell 1	0	Gt, Sh	5.05	0.10	0.19	0.004	0.73	6.9	54.73	17.44	51.57	7.6	YR	5.3	8.8	3.88	278	1.46
Bell 2	450	Sh, Gt	5.03	0.03	0.05	0.003	0.90	5.6	63.67	13.62	49.59	8.5	YR	6.3	8.1	3.83	283	1.35
Bell 3	900	Gt, Sh	5.77	0.09	0.17	0.004	0.71	8.1	56.68	13.74	48.98	8.8	YR	5.6	8.1	3.80	286	1.35
Big Mnt 1	0	Gt, Sh	4.64	0.05	0.27	0.003	0.75	6.2	63.65	12.87	55.31	9.3	YR	6.3	8.8	4.04	827	5.20
Big Mnt 2	100	Sh, Gt	5.33	0.01	0.04	0.004	0.97	5.5	57.76	12.77	51.58	9.3	YR	5.7	8.3	3.42	827	5.20
Big Mnt 3	125	Gt, Sh	5.12	0.01	0.03	0.003	1.04	4.9	61.74	12.21	54.06	9.5	YR	6.1	8.6	3.16	827	5.10
Colket	0	Sh, Gt	5.05	0.21	0.14	0.003	0.61	8.3	47.44	20.77	42.86	5.9	YR	4.6	7.9	5.79	417	1.56
Hegins	0	ALHS	0.41	0.63	8.92	0.002	1.04	0.4	72.73	2.81	17.12	0.1	Y	7.2	2.6	6.86	502	1.87
Markson	0	Gt, Qz	5.02	0.05	0.03	0.004	0.58	8.6	62.75	13.41	60.24	9.4	YR	6.2	9.6	3.45	804	5.31
Middle Creek 1	0	Sh, Qz	4.65	0.16	1.74	0.002	0.73	6.4	58.28	14.27	42.80	7.9	YR	5.7	7.2	5.10	256	0.97
Otto 1	0	2-line Fh	4.71	0.76	2.56	0.002	0.38	12.3	58.88	15.95	41.98	7.1	YR	5.8	7.3	5.70	570	2.39
Otto 2	225	2-line Fh	5.72	1.19	1.59	0.051	0.27	21.2	58.04	17.37	44.53	6.9	YR	5.7	7.8	5.70	570	2.39
Otto 3	470	6-line Fh	4.96	0.95	1.46	0.004	0.21	23.7	54.38	18.00	41.57	6.4	YR	5.3	7.4	5.68	568	2.39
Silver Creek 1	0	Fh(?)	4.48	0.92	3.00	0.002	0.51	8.7	56.75	9.67	35.76	9.0	YR	5.6	5.7	5.91	543	2.50
Silver Creek 2	120	2–3 line Fh	5.32	0.66	1.44	0.003	0.49	10.9	52.28	17.91	40.60	6.4	YR	5.1	7.2	6.03	542	2.29
Silver Creek 3	220	Fh, Gt	6.91	0.71	1.18	0.006	0.46	15.0	46.44	14.89	33.37	6.7	YR	4.5	5.9	6.31	537	2.39
Tracy 1	0	Gt, Lp, Fh	5.01	0.40	0.10	0.005	0.14	36.4	54.44	19.55	45.50	6.4	YR	6.3	9.1	5.79	619	2.50
Tracy 2	200	5-line Fh	5.32	0.48	0.04	0.061	0.13	39.6	45.8	22.3	41.52	5.2	YR	4.5	7.9	6.28	609	2.39
Tracy 3	350	6-line Fh	5.32	0.57	0.07	0.233	0.12	44.3	43.65	18.96	37.09	5.8	YR	4.3	6.9	6.58	603	2.39
Valley View	0	5–6 line Fh	5.22	0.56	0.29	0.007	0.21	25.1	50.46	20.14	42.35	6.0	YR	4.9	7.8	6.03	238	1.01

<sup>a</sup> Lp = lepidocrocite, Fh = ferrihydrite, Sh = schwertmannite, Gt = goethite, ALHS = amorphous aluminum hydroxysulfate compound.

Red–Green–Blue (RGB) was accomplished using Photoshop (Adobe systems).

To further compare their spectral properties, a spectral angle difference technique was applied to the color measurements (Kruse et al., 1993a). The spectrum of a material can be expressed as a vector in space whose dimensions are equal to the number of spectral bands. For example, the RGB color space has 3 dimensions, whereas a hyperspectral sensor could have more than 100 dimensions. The spectral similarity between the sediment sample and a reference mineral was determined by computing the angle between the two spectra in RGB color space (Van der Meer, 1997). The similarity of two or more spectra was then calculated using the arc-cosine of the dot product, or theta, expressed as:

$$\theta = \cos^{-1} \frac{t \bullet r}{\| \vec{t} \| \bullet \| \vec{r} \|}$$

where  $t$  was the sample spectrum and  $r$  was the reference spectrum.

Materials that were spectrally similar to the reference had a dot product of 1, and low theta angles. Dissimilar materials had high theta angles.

### 2.5.3. Spectroscopic analysis

Diffuse reflectance spectroscopy in the visible to near infrared range (VNIR) was performed using an analytical spectral devices (ASD) FieldSpec FR portable spectroradiometer at the USGS Spectroscopy laboratory in Denver, Colorado. Freeze-dried and ground samples were placed on weighing paper and illuminated with an industry standard optically pure white light. The ASD FieldSpec FR is equipped with a fiber optic cable that was held close to the sample at about a 30° angle. All samples were step scanned from 350 to 2500 nm in increments of 1 nm with a 34 ms integration time.

Red and yellow Fe oxides absorb in the UV and reflect strongly in the VNIR (Cornell and Schwertmann, 1996). Absorption effects in the VNIR are a result of 3 types of electronic transitions: crystal or ligand field transitions, magnetic coupling of Fe(III) ions, and O-metal charge transfer effects (Sherman and Waite, 1985). All Fe oxides have absorption features that can be resolved by removing the continuum in a spectrum. The continuum can be thought of as the background, and features of interest are superimposed onto this background absorption (Clark and Roush, 1984). The VNIR diffuse reflectance spectrum of a sample generally has a sloping background due to scattering and the additive effect of optical constants (Clark and Roush, 1984). Removal of the background was accomplished by using the spectrum processing routines (SpecPR) code developed at the USGS spectroscopy laboratory (Clark et al., 1990). This code fitted a convex-hull over the top of each spectrum using linear segments that connected

local maxima (Kruse et al., 1993b). The original spectrum was divided by the continuum-line to produce a continuum-removed spectrum. This procedure isolated the absorption band centers and allowed these features to be easily compared with other diffuse reflectance spectra (Clark, 1999).

### 2.5.4. Sediment chemistry

Chemical composition of the sediments was obtained by selective dissolution of the freeze-dried solids in cold 5 M HCL (Winland et al., 1991). Iron, Al, Mn, Pb, As, S, and Se in the acid dissolution extracts were measured using a Perkin Elmer inductively-coupled plasma optical emission spectrometer (ICP-OES). Total S content of the sediments was measured using a Leco Model 521 induction furnace.

### 2.5.5. Mineral synthesis

Samples of goethite, schwertmannite, and ferrihydrite were synthesized for comparison to the field samples using the procedures of Schwertmann and Cornell (1991). The synthetic samples were subjected to the same analyses as the natural samples.

## 3. Results and discussion

### 3.1. Geochemistry of mine drainage waters

The aqueous chemistry of the mine drainage waters (Table 1) was consistent with previously published data for these and other sites in the Anthracite region of eastern Pennsylvania (Cravotta et al., 1999; Wood, 1996). The pH of the source waters ranged between 3.2 and 6.9, indicating a diversity of geochemical conditions. Despite aeration, the pH and other characteristics of the water sampled at locations downstream from the outfall changed little; pH varied within 1 unit and concentrations of solutes differed by 10% or less. Sulfate was the dominant anion, ranging from 0.97 to 5.31 mmol/l. Iron and Mn were elevated (13  $\mu\text{mol/l}$ ) in most samples, whereas Al was elevated only in low pH samples. A relatively high SC (238–827  $\mu\text{S/cm}$ ) was associated with both low and high pH samples and reflects elevated concentrations of  $\text{SO}_4$ . Sites characterized by low SC and  $\text{SO}_4$  imply the mine drainage had been diluted by non-degraded surface or groundwater. Low SC and  $\text{SO}_4$  could also imply that acid-forming reactions were diminished due to limited exposure of pyrite to  $\text{O}_2$  in flooded mines.

Values of  $\log_a \text{Fe}^{3+}$  for the drainage waters were inversely correlated with pH as would be expected where Fe minerals are actively precipitating. Solubility lines calculated for goethite, ferrihydrite, and schwertmannite assuming constant  $\text{pSO}_4$  (Fig. 2a) (Yu et al., 1999; Bigham et al., 1996) show that most of the mine

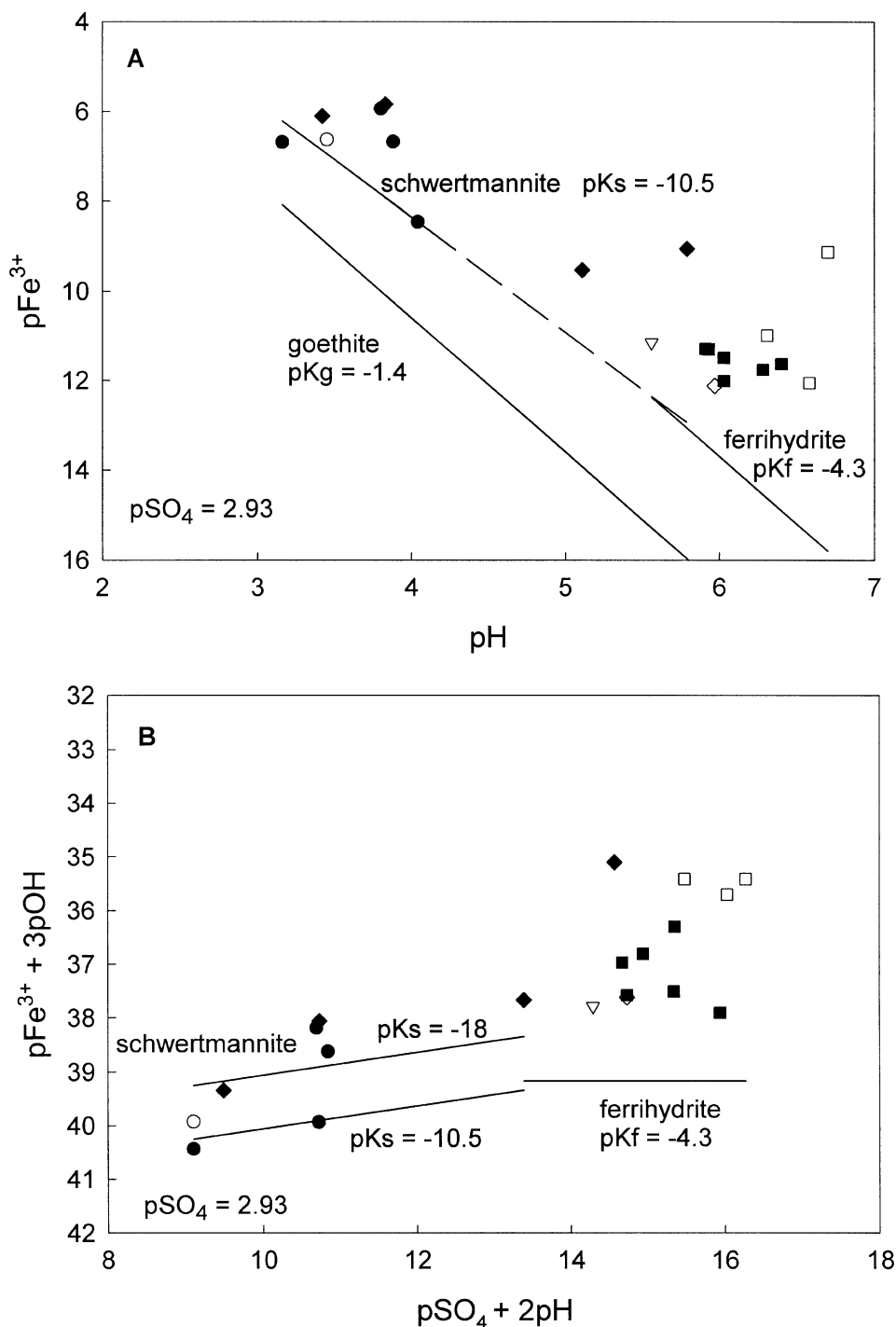


Fig. 2. Activity of  $\text{Fe}^{3+}$  relative to pH. Activity computed using WATEQ4F (Ball and Nordstrom, 1991). Solubility lines are as follows: Gt = goethite ( $\log a_{\text{Fe}^{3+}} = 1.4\text{--}3$  pH), Fh = ferrihydrite ( $\log a_{\text{Fe}^{3+}} = 4.3\text{--}3$  pH), and Sh = schwertmannite ( $\log a_{\text{Fe}^{3+}} = 2.83\text{--}2.6$  pH). Solubility lines calculated using an average  $\log a_{\text{SO}_4^{2-}} = -2.93$ , and  $K_{\text{so}}$  values for Gt, Fh, and Sh of  $-1.40$ ,  $-4.3$ , and  $-10.5$  respectively (Yu et al., 1999). (b) Plot of  $(p\text{SO}_4 + 2p\text{H})$  versus  $(p\text{Fe} + 3p\text{PH})$ . Solubility lines for schwertmannite were calculated using  $pK_{\text{so}}$  values of  $-18$  (Bigham et al., 1996) and  $-10.5$  (Yu et al., 1999). Symbols are:  $\circ$ —goethite (gt),  $\bullet$ —gt + schwertmannite (sh) with gt dominant,  $\blacklozenge$ —sh + gt with sh dominant,  $\blacksquare$ —ferrihydrite (fh),  $\square$ —fh + gt with fh dominant,  $\diamond$ —gt + lepidocrocite + fh with gt dominant,  $\nabla$ —sh + fh with sh dominant.

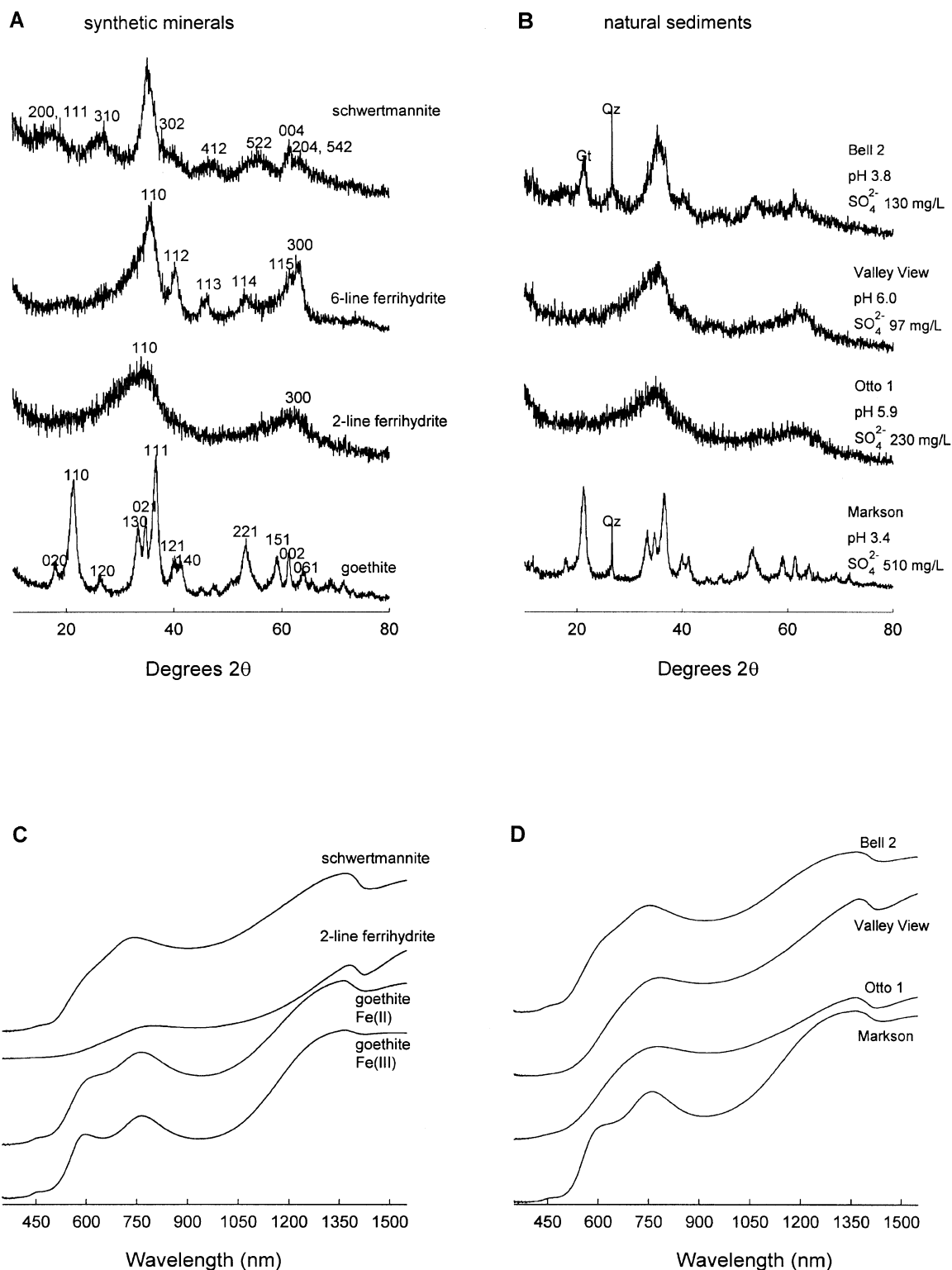


Fig. 3. X-ray diffraction patterns and reflectance spectra for laboratory synthesized minerals and natural sediments collected for this study. (a and b) X-ray diffraction pattern; Qz = quartz, Gt = goethite; Miller indices given for synthetic minerals. (c and d) Reflectance spectra in the UV-vis-near IR range. Reflectance spectra offset by 0.2 for clarity.

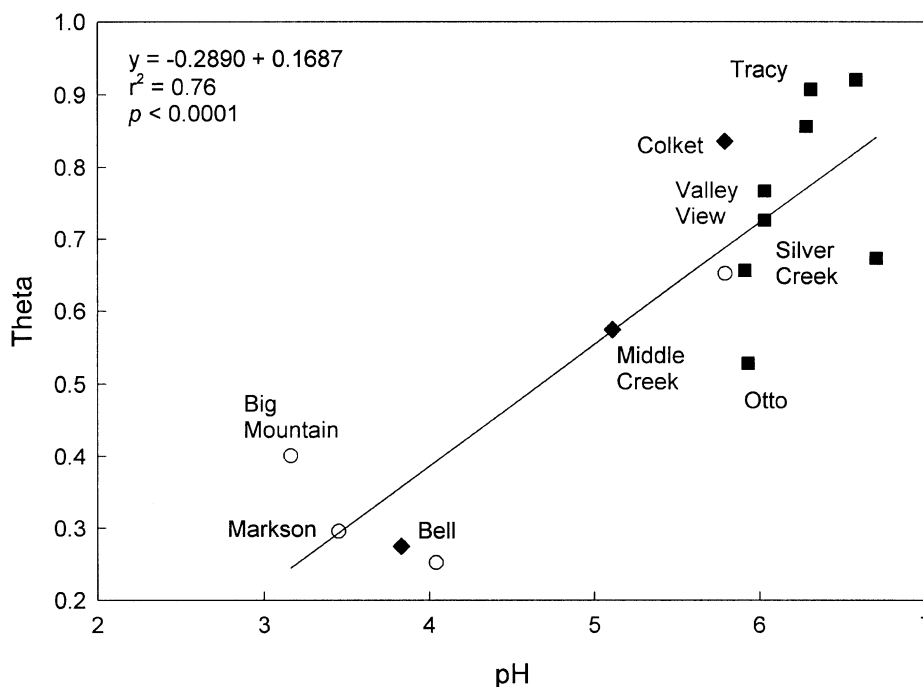


Fig. 4. Sediment spectral angle differences in relation to source water pH. Synthetic goethite was used as the end-member reference mineral to compute theta. Symbols are: ■—ferrihydrite, ○—goethite, ◆—schwertmannite.

waters were supersaturated with respect to these minerals. This apparent supersaturation may be due to instability of schwertmannite (sh) and ferrihydrite (fh) with respect to goethite (gt) (Bigham et al., 1996). Another possible cause of supersaturation is that some colloidal particles passed through the 0.45- $\mu\text{m}$  filters and were analyzed with the dissolved fractions (Kimball et al., 1995). The inclusion of  $\text{SO}_4$  activity as a variable as recommended by Yu et al. (1999) (Fig. 2b) indicated that most sh-containing samples were at or near saturation depending on the apparent solubility product selected (−18 vs. −10.5). Clearly, sh and fh tended to precipitate under different geochemical regimes.

### 3.2. Sediment mineralogy and composition

The sediment mineralogy varied with pH of the drainage waters (Table 1). Schwertmannite was formed in pH environments of 3.1–5.8, whereas ferrihydrite was precipitated from waters having pH values of 5.7 and above. In the latter situation, two-line ferrihydrite dominated the sediments nearest the mine drainage source, while 5–6 line ferrihydrite, a more crystalline phase of the mineral, was found in sediments collected further downstream (e.g. Otto mine). Goethite was found throughout the pH range of the sample sites, from 3.4 to 6.7, and was the dominant phase at the Markson mine. Lepidocrocite was found in only one sediment sample collected at an airshaft discharging

anoxic water (Tracy 1). A white, Al hydroxysulfate compound that yielded 3 broad XRD bands at 4.4, 2.2, and 1.46  $\text{\AA}$  was present at the Hegins site. This compound was formed by mixing near-neutral water with acidic drainage waters that were high in dissolved Al and  $\text{SO}_4$  (Nordstrom and Alpers, 1999).

The sediments can also be grouped according to their total Fe to S ( $\text{Fe}_{\text{tot}}/\text{S}_{\text{tot}}$ ) molar ratios (Table 1). Sediments formed in low pH waters generally had  $\text{Fe}_{\text{tot}}/\text{S}_{\text{tot}}$  ratios of 5.6–8.6 with a mean of 6.4 and were composed of schwertmannite and goethite. Schwertmannite-rich sediments had the lowest ratios, which can be attributed to structural and surface sorbed  $\text{SO}_4$  (Bigham et al., 1996). Sediments from circumneutral pH waters had  $\text{Fe}_{\text{tot}}/\text{S}_{\text{tot}}$  ratios ranging from 10.9 to 44.3 with a mean of 24.4 and were ferrihydritic in composition. As previously reported for natural ferrihydrites (e.g. Winland et al., 1991), those samples contained 50–100 times more Si than those dominated by goethite or schwertmannite. Manganese was not a major component in any of the precipitates (Table 1). The Hegins site, which had sediments composed of an Al hydroxysulfate compound, had a  $\text{Fe}_{\text{tot}}/\text{S}_{\text{tot}}$  ratio of 0.4 and an  $\text{Al}_{\text{tot}}/\text{S}_{\text{tot}}$  ratio of 8.6.

Several of the natural samples were mineralogically pure, and could be viewed as end-members of the mineral spectrum associated with mine drainage waters. The purity of the natural samples was confirmed by comparison of their XRD profiles and reflectance spectra with those of the synthetic specimens (Fig. 3a and b).

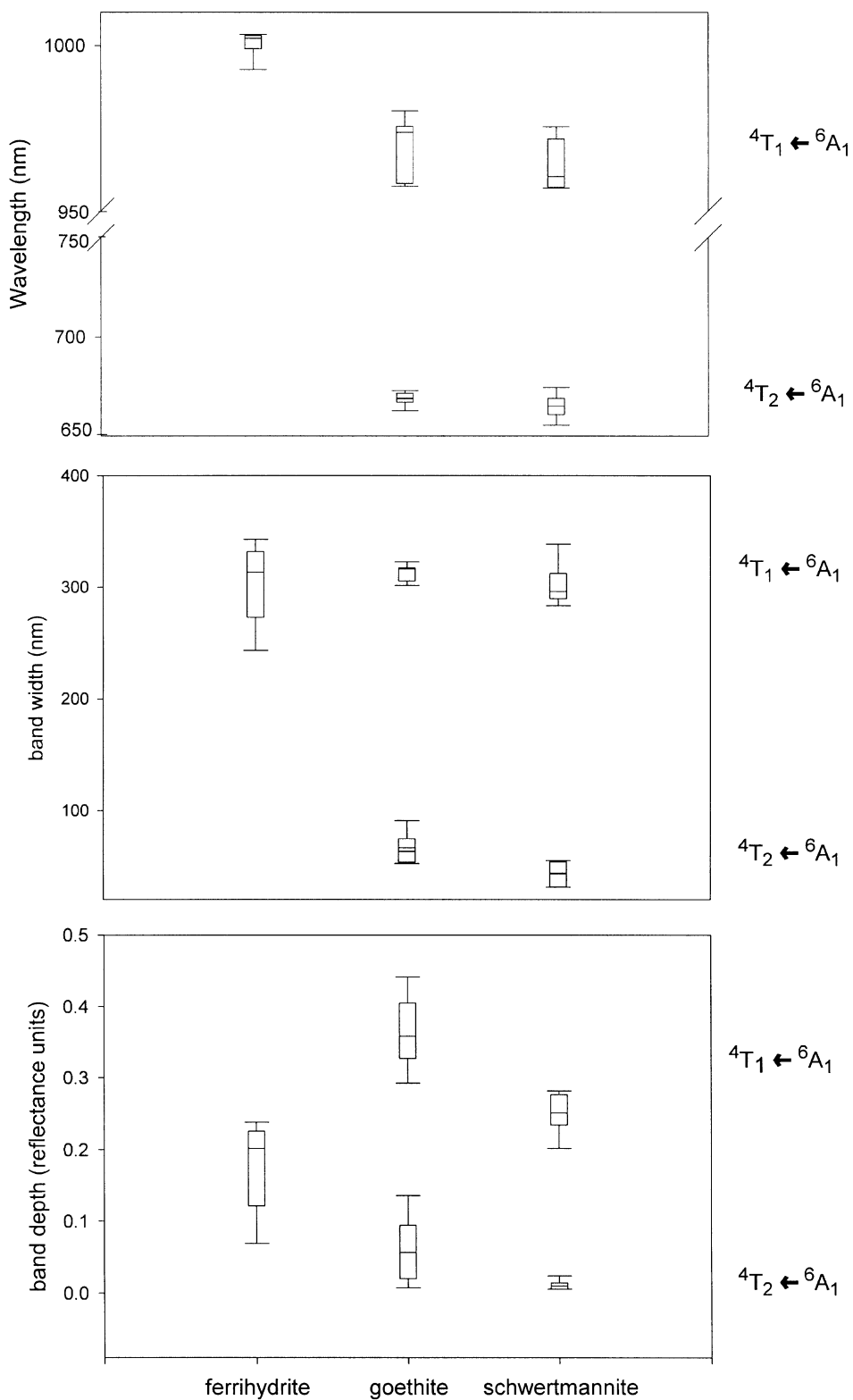


Fig. 5. Median and range of the crystal field band center, width and depth as determined by continuum-removed band center analysis. Measurements for band width and band depth were calculated at the band center.

### 3.3. Spectral analysis

Sediments containing significant amounts of ferrihydrite were redder and darker than the goethitic or schwertmannitic sediments (Table 1). Therefore, several spectral techniques may have potential for relating the reflectance characteristics of mine drainage precipitates to the general quality of the effluent waters.

#### 3.3.1. Spectral angle difference

The theta angle was calculated to predict source water pH (Fig. 4) using synthetic goethite as the reference. Sediments forming in low pH drainage waters generally have high goethite and/or schwertmannite contents and thus are spectrally similar to the reference. Their resulting dot products are near unity, and theta angles approach zero. Near neutral pH source waters produced mainly ferrihydrite and had high theta angles when compared to the goethite reference. The grouping of the precipitates reinforces the relationship between sediment color and source water pH.

#### 3.3.2. Visible to near infrared diffuse reflectance analysis

Diffuse reflectance spectroscopy of the natural precipitates also indicated a spectral separation between sediments composed of goethite and/or schwertmannite and ferrihydrite rich sediments. A strong reflectance feature can be observed for Fe oxides between 600 and 1000 nm (Fig. 3c and d). For sediments containing

mostly goethite, e.g. Markson, the peak reflectance was at 759 to 761 nm. The peak reflectance for ferrihydritic sediments, e.g. Otto and Valley View, was between 779 and 787 nm. For sediments containing schwertmannite (e.g. Bell) the reflectance peak shifted to lower wavelengths between 755 and 757 nm.

#### 3.3.3. Spectral feature comparison by continuum removal

Absorbance features for the synthetic minerals and natural sediment samples are given in Fig. 5, where the band center differences for goethitic/schwertmannitic and ferrihydritic samples can readily be seen. Continuum removal isolated the absorption band occurring from an electron pair transition (EPT)  $2(^4T_1) \leftarrow 2(^6A_1)$  (479–499 nm) in the synthetic and natural goethites at approximately 487 nm (mean) (Williams, 1999). The  $4T_1 \leftarrow 6A_1$  (900–1000 nm) band center mean for synthetic and natural goethites was 968.0 nm. Band centers for goethite and schwertmannite could not be resolved. By contrast, band centers for the ferrihydrites ranged from 1003 to 990 nm with a mean of 995.8 nm and were easily distinguished. As ferrihydrite crystallinity increased from the 2-line to the 6-line phase, a downward shift to 998 nm was seen in Tracy-3, and a shift to 990 nm occurred in Otto-3. The lepidocrocite-ferrihydrite sample collected from the Tracy mine airshaft had a band center at 1003.4 nm (Williams, 1999). A recent study using second-derivative reflectance spectroscopy of synthetic and

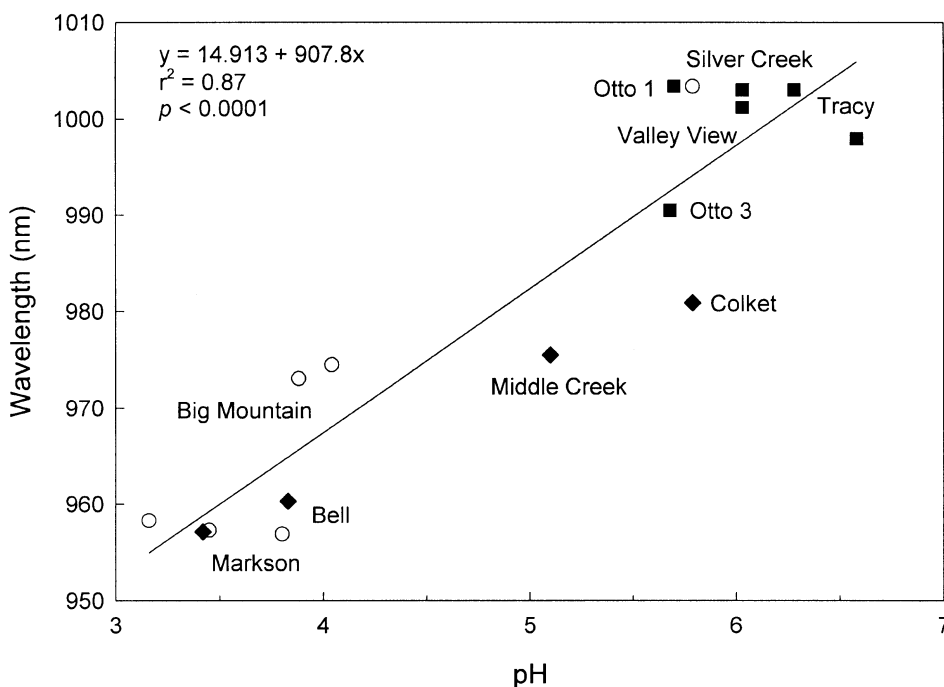


Fig. 6. Adsorption band positions corresponding to the  $4T_1 \leftarrow 6A_1$  crystal field transition relative to pH for sediments collected in this study. Symbols are: ■—ferrihydrite, ○—goethite, ◆—schwertmannite.

natural Fe oxides reported similar band center positions (Schienost et al., 1998).

Mineral identification using band center analysis proved to be the most accurate method for predicting mine drainage pH. The relationship between source water pH and the  ${}^4T_1 \leftarrow {}^6A_1$  absorption band-center had

an  $r^2$  of 0.87 (Fig. 6). Additional influences of the geochemical environment on the diffuse reflectance properties of the precipitates can be seen in the absorption band centers, and the band depths and widths as defined by full width at half maximum (fwhm) (Fig. 5). Cornell and Schwertmann (1996) reported that goethites synthesized

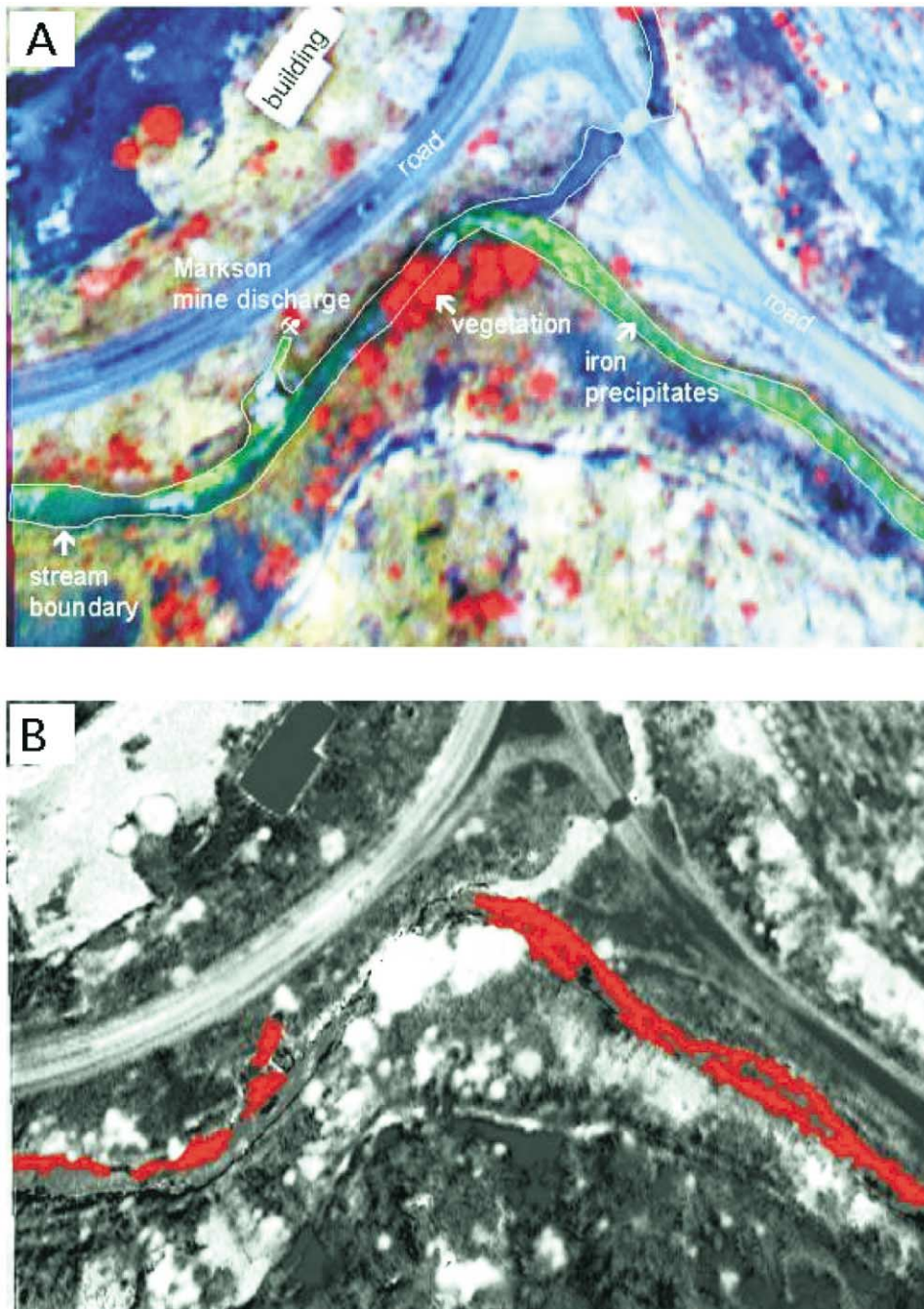


Fig. 7. (a) False color composite DMSV image of the Markson mine site. (b) Spectral angle mapper (SAM) classification image of the site. Colored areas indicate goethitic sediments.

from Fe(III) contain well crystallized particles having surface areas of about 20 m<sup>2</sup>/g, whereas synthesis using Fe(II) yields precipitates of low crystallinity and surface areas of around 80 m<sup>2</sup>/g. In the present study, crystallinity affected the band depth for the  ${}^4T_1 \leftarrow {}^6A_1$  and the  ${}^4T_2 \leftarrow {}^6A_1$  and  $2({}^4T_1) \leftarrow 2({}^6A_1)$  transitions. Goethite synthesized using the Fe(II) method had an EPT band center at 485.3 nm, a  ${}^4T_2 \leftarrow {}^6A_1$  at 666.9 nm, and a  ${}^4T_1 \leftarrow {}^6A_1$  at 975.6 nm, versus 491.3, 673.0, and 980.8 nm, respectively, for the Fe(III) method. Band depths for the Fe(II) method samples had an EPT of 0.6541, a  ${}^4T_2 \leftarrow {}^6A_1$  of 0.0942, and a  ${}^4T_1 \leftarrow {}^6A_1$  of 0.4046, versus 0.7808, 0.1405, and 0.4458 nm, respectively for the Fe(III) method. This shift (and band depth decrease) was even more pronounced in the natural goethites. The  ${}^4T_1 \leftarrow {}^6A_1$  transition for the natural goethites, excluding the Markson mine goethite, had a band center mean of 667.2 nm and a band depth mean of 0.015 and compares well with goethite formed by Fe(II) synthesis. The well crystalline end-member goethite from the Markson mine shows a more distinct absorption band (band depth of 0.0853) and compares well with the sample synthesized by the Fe(III) method (Fig. 3c and d). The natural goethites were formed in the presence of significant amounts of dissolved SO<sub>4</sub>, Al, and other ions that can retard crystal growth and yield precipitates of low crystallinity (Cornell and Schwertmann, 1996). The low crystallinity of natural ferrihydrites can also be seen in the small band depths of the Valley View precipitate (Fig. 3d).

The  ${}^4T_2 \leftarrow {}^6A_1$  single electron transition (650–680 nm) can be useful for separating ferrihydrite from goethite or schwertmannite rich sediments because ferrihydrite usually does not have a detectable absorption band for this transition (Fig. 1 in Scheinost et al., 1998). The  ${}^4T_2 \leftarrow {}^6A_1$  transition can also be used in separating goethitic versus schwertmannitic sediments. This transition is less pronounced for schwertmannite relative to goethite. The band widths and depths for this transition are narrower and shallower, respectively, for schwertmannite as compared to goethite (Fig. 5).

#### 3.4. Remote sensing of mine drainage minerals

In a trial study funded by the US EPA Advanced Measurement Initiative (AMI), narrow band multispectral imagery was used to investigate the use of remote sensing to detect mine drainage minerals and the associated biogeochemical conditions (E.I Robbins and J.E. Anderson, 1998, written communication). Airborne DSMV imagery was obtained for several sites in the study region. Chemical precipitates were apparent in a scene acquired over the Markson mine site (Fig. 7a). This image is a false color composite using the 550, 650 and 750 nm bands (Lillesand and Keifer, 1994). The spatial resolution (pixel size) of the image is approximately

70 cm. The mine drainage precipitates reflect in the 750 and 650 nm bands and appear bright yellowish-green in the image. Water absorbs light energy, especially in the infra-red and appears dark in the image.

Spectral angle mapping (SAM) was applied to the image using in-scene materials of known mineralogy, as determined in the laboratory, as reference spectra (Williams, 1999; Kruse et al., 1993a). Goethitic sediments from a pool at the Markson mine were identified in the image and were used to develop reference spectra. The output of the SAM routine is a data array (image) that contains the calculated theta values. The pixels with the lowest theta values are materials that are spectrally similar to the reference material and are classified as goethitic sediments (mixture of goethite and schwertmannite) in the resulting thematic map (Fig. 7b). The chemical precipitates present at this site formed under low pH and moderate to high dissolved SO<sub>4</sub> concentrations.

#### 4. Conclusions

The pH of mine drainage and the mineralogy of Fe minerals formed at mine discharge sites in the Anthracite region were found to be related. In general, schwertmannite dominated for low pH (<4) conditions and ferrihydrite dominated for near-neutral pH (>5.5) conditions. Schwertmannite was also present in several samples occurring under near-neutral conditions (pH 5.6–5.8). Goethite was found throughout the range of conditions but was most abundant in low pH systems. Because these minerals have distinctive color and spectral reflectance, these measurements can be useful to distinguish acidic and near-neutral mine drainage. Although dissolved SO<sub>4</sub> concentrations were highly variable in the acidic waters, elevated SO<sub>4</sub> concentration (>100 mg/l) can be deduced from the presence of schwertmannite in the chemical precipitates.

Narrow band multispectral remote sensing can be useful for identification and mapping of mineralogy and can help define the pH of associated mine drainage. Multispectral systems, however, are limited in accuracy due to the lack of numerous and continuous spectral bands. Advanced remote sensing technologies, such as hyperspectral or imaging spectrometers allow for more accurate mineralogical identification and should provide better estimates of water quality in complex aquatic systems. Nevertheless, more research is needed to resolve uncertainties about the application of remote sensing for the characterization of mine drainage chemistry.

#### Acknowledgements

The authors wish to acknowledge E.I Robbins and K.A. Balcialskas (US Geological Survey) and E. Terrance

Slonecker (US Environmental Protection Agency) for their assistance and Franklin Schwartz (The Ohio State University) for funding support through the US Department of Defense Environmental Restoration Fellowship. The US Environmental Protection Agency through its Office of Research and Development partially funded and collaborated in the research described here. It has been subjected to Agency review and approved for publication. Mention of trade names or commercial products does not constitute an endorsement or recommendation for use.

## References

- Albers, P.H., Camardese, M.B., 1993. Effects of acidification on metal accumulation by aquatic plants and invertebrates. 1. Constructed wetlands. *Environ. Tox. Chem.* 12, 959–967.
- Anderson, J.E., Robbins, E.I., 1998. Spectral reflectance and detection of iron-oxide precipitates associated with acidic mine drainage. *Photogrammetric Eng. Remote Sens.* 64, 1201–1208.
- Ball, J.W., Nordstrom, D.K., 1991. Users manual for WATEQ4F, with revised thermodynamic database and test cases for calculation speciation of major, trace and redox elements in natural waters: US Geol. Surv., Open File Rep. 91–83.
- Bigham, J.M., Schwertmann, U., Traina, S.J., Winland, R.L., Wolf, M., 1996. Schwertmannite and the chemical modeling of iron in acid sulfate waters. *Geochim. Cosmochim. Acta* 60, 2111–2121.
- Bigham, J.M., Murad, E., 1997. Mineralogy of ochre deposits formed by the oxidation of iron sulfide minerals. In: Auerswald, K., Stanjek, H., Bigham, J.M. (Eds.), *Advances in GeoEcology* 30. Catena Verlag, Reiskirchen, pp. 193–225.
- Clark, R.N., Roush, T.L., 1984. Reflectance spectroscopy: quantitative analysis techniques for remote sensing applications. *J. Geophys. Res.* 89, 6329–6340.
- Clark, R.N., Gallagher, A.J., Swayze, G.A., 1990. Material absorption band depth mapping of imaging spectrometer data using a complete band shape least-squares fit with library reference spectra. *Proceedings of the Second Airborne Visible/Infrared Imaging Spectrometer (AVIRIS) Workshop*. JPL Publication 90–54.
- Clark, R.N., 1999. Spectroscopy of rocks and minerals, and principles of spectroscopy. In: Rencz, A.N. (Ed.), *Remote Sensing for the Earth Sciences*. American Society for Photogrammetry and Remote Sensing, Wiley, pp. 3–58.
- Cornell, R.M., Schwertmann, U., 1996. *The Iron Oxides: Structure, Properties, Reactions, Occurrence and Uses*. Verlag Chemie, Weinheim.
- Cravotta, C.A., III, Brady, K.B.C., Rose, A.W., Douds, J.B., 1999. Frequency distribution of the pH of coal-mine drainage in Pennsylvania. In: Morganwalp, D.W., Buxton, H. (Eds.), *US Geological Survey Toxic Substances Hydrology Program*. USGS Water Resour. Invest. Rep. 99–4018A, pp. 313–324.
- Durlin, R.R., Schaffstall, W.P., 1998a. Water Resources Data for Pennsylvania, Water Year 1997; Vol. 2, Susquehanna and Potomac River Basins. US Geol. Surv. Water Data Rep. PA-98–2.
- Durlin, R.R., Schaffstall, W.P., 1998b. Water Resources Data for Pennsylvania, Water Year 1997; Vol. 1, Delaware River Basins. US Geol. Surv. Water Data Rep. PA-98–1.
- Fishman, M.J., Friedman, L.C. (Eds.), 1989. *Methods for Determination of Inorganic Substances in Water and Fluvial Sediments* US Geol. Surv. Techniques of Water-Resources Investigations, Book 5, (Chapter A1).
- Gray, N.F., 1997. Environmental impact and remediation of acid mine drainage: a management problem. *Environ. Geol.* 30, 62–71.
- Kimball, B.A., Callender, E., Axtmann, E.U., 1995. Effects of colloids on metal transport in a river receiving acid mine drainage, upper Arkansas River, Colorado, U.S.A.. *Appl. Geochem.* 10, 285–306.
- Kruse, F.A., Lefkoff, A.B., Boardman, J.W., Heidebrecht, K.B., Shapiro, A.T., Barloon, P.J., Goetz, A.F.H., 1993a. The spectral image processing system (SIPS)—interactive visualization and analysis of imaging spectrometer data. *Remote Sens. Environ.* 44, 145–163.
- Kruse, F.A., Lefkoff, A.B., Dietz, J.B., 1993b. Expert system-based mineral mapping in northern Death Valley, California and Nevada using the airborne visible/infrared imaging spectrometer (AVIRIS). *Remote Sens. Environ.* 44, 309–336.
- Lillesand, T.M., Keifer, R.W., 1994. *Remote Sensing and Image Interpretation*. Wiley, New York.
- Nordstrom, D.K., 1977. Thermochemical redox equilibria of Zobell's solution. *Geochim. Cosmochim. Acta* 41, 1835–1841.
- Nordstrom, D.K., Alpers, C.N., 1999. Geochemistry of acid mine waters. In: Plumlee, G.S., Logsdon, M.J. (Eds.), *The Environmental Geochemistry Of Mineral Deposits, Part A: Processes, Techniques, and Health Issues*. Rev. Econ. Geol., Vol. 6A. Society of Economic Geologists, pp. 133–160 (Chapter 6).
- Rantz, S.E., 1982. Measurement and computation of streamflow. Measurement of stage and discharge. USGS Water-Supply Paper 2175, Vol. 1.
- Rose, A.W., Cravotta C.A. III, 1998. Geochemistry of coal mine drainage. In: Brady, K.B.C., Smith, M.W., Schueck, J. (Eds.), *Coal Mine Drainage Prediction and Prevention in Pennsylvania*. Pennsylvania Dept. of Environmental Protection, 5600-Bk-DEP2256, pp. 1.1–1.22.
- Robbins, E.I., Anderson, J.E., Cravotta, C.A., III, Nord, G.L., Slonecker, E.T., 2000. Multispectral signature variations in acidic versus near-neutral contaminated coal mine drainage in Pennsylvania. In: *Proc. Int. Conf. on Acid Rock Drainage*, Littleton, Co., Soc. Mining, Metallurgy, and Exploration, Inc., Vol. 2, pp. 1551–1559.
- Rosseland, B.O., Eldhuset, T.D., Staurnes, M., 1990. The environmental effects of aluminum. *Environ. Geochem. Health* 12, 17–27.
- Scheinost, A.C., Chavernas, A., Barron, V., Torrent, J., 1998. Use and limitations of second-derivative diffuse reflectance spectroscopy in the visible to near-infrared range to identify and quantify Fe oxide minerals in soils. *Clays Clay Miner.* 46, 528–536.
- Schwertmann, U., Cornell, R.M., 1991. *Iron Oxides in the Laboratory: Preparation and Characterization*. VCH, Weinheim.
- Sengupta, M., 1993. *Environmental Impacts of Mining: Monitoring, Restoration, and Control*. Lewis Publishers, Boca Raton.

- Sherman, D.M., Waite, T.D., 1985. Electronic spectra of Fe<sup>3+</sup> oxides and oxide hydroxides in the near IR to near UV. *Am. Min.* 70, 1262–1269.
- Swayze, G.A., Smith, K.M., Clark, R.N., Sutley, S.J., Pearson, R.M., Vance, J.S., Hageman, P.L., Briggs, P.H., Meier, A.L., Singleton, M.J., Roth, S., 2000a. Using imaging spectroscopy to map acidic mine waste. *Environ. Sci. Technol.* 34, 47–54.
- Swayze, G.A., Smith, K.M., Clark, R.N., Sutley, S.J., 2000b. Imaging spectroscopy—a new screening tool for mapping acidic mine waste. *Proc. Int. Conf. on Acid Rock Drainage*, Littleton, Co., Soc. Mining, Metallurgy, and Exploration, Inc., Vol. 2, pp. 1531–1539.
- Van der Meer, F., 1997. Mineral mapping and Landsat thematic mapper image classification using spectral unmixing. *Geocarto Int.* 12, 27–40.
- Way, J.H., 2000. Appalachian Mountain section of the Ridge and Valley province. In: Schultz, C.H. (Ed.), *Pennsylvania Geol. Survey.*, 4th ser. Spec. Publ. 1, pp. 352–361.
- Wilde, F.D., Radtke, D.B., Gibs, J., Iwatsubo, R.T., 1998. National field manual for the collection of water-quality data. *US Geol. Sur. Techniques of Water Resources Investigations*, Book 9, Handbooks for Water-Quality Investigations, variously paged (<http://water.usgs.gov/owq/FieldManual>).
- Williams, D.J., 1999. Spectral Reflectance as an Indicator of Water Quality in Streams Impacted by Mine Drainage. MS thesis. Ohio State Univ., Columbus, OH.
- Winland, R.L., Traina, S.J., Bigham, J.M., 1991. Chemical composition of ochreous precipitates from Ohio coal mine drainage. *J. Environ. Qual.* 20, 452–460.
- Wood, G.H., Kehn, T.M., Eggleston, J.R., 1986. Deposition and structural history of the Pennsylvania Anthracite region. In: Lyons, P.C., Rice, C.L., (Eds.), *Paleoenvironmental and Tectonic Controls in Coal-forming Basins of the United States*, *Geol. Soc. Am. Spec. Pap.* 210, pp. 31–47.
- Wood, C.R., 1996. Water quality of large discharges from mines in the anthracite region of eastern Pennsylvania. *USGS Water-Resour. Invest. Rep.* 95–4243.
- Wood, W.W., 1976. Guidelines for collection and field analysis of ground-water samples for selected unstable constituents. *USGS Techniques of Water-Resource Investigations*, chapter D2.
- Yu, J.Y., Heo, B., Choi, I.K., Cho, J.P., Chang, H.W., 1999. Apparent solubilities of schwertmannite and ferrihydrite in natural stream waters polluted by mine drainage. *Geochim. Cosmochim. Acta* 63, 3407–3416.